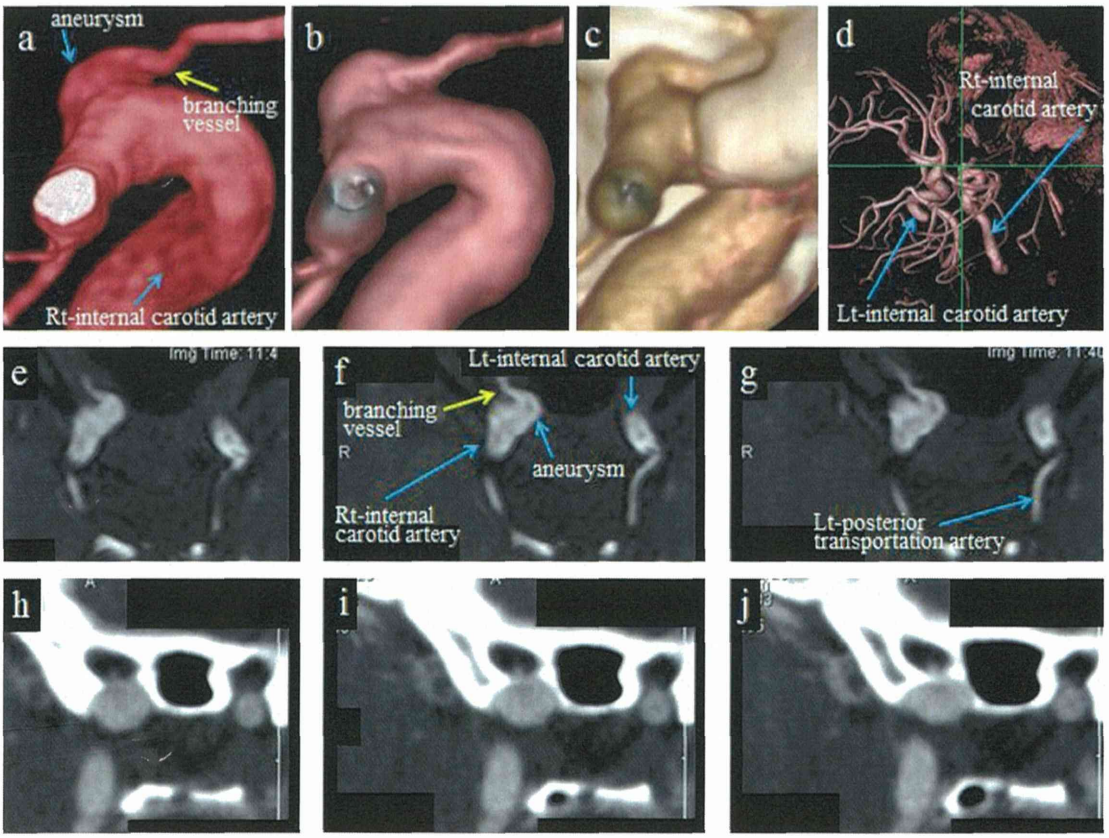

Fig. 3. False negative on 'CTA-VR + source images' and true positive on 'MRA-VR + source images' observed in patient 20. (a) VR-rotational DSA; (b) MRA-VR; (c) CTA-VR; (d) global image of (b). The aspect is the same in (a)–(c) and is shown in (d). (e)–(g) MRA source images. (h)–(j) CTA source images. The yellow arrows indicate a branch vessel arising from the aneurysm sac, which is positioned at the center of image d. For subfigures (e)–(g) and (h)–(j), the image slices run superior to inferior, from left to right. (For interpretation of the references to color in this figure legend, the reader is referred to the web version of the article.)

time, and coverage for the evaluation of cerebrovascular diseases. The superior performance of MRA with a 3-tesla MR system compared with that of a 1.5-tesla MR system was demonstrated in a previous study [14]. The utility of MRA-VR and the resultant improved image quality in 3-tesla MR were also reported previously; in addition, MRA-VR has been used as a screening tool for three-dimensional spatial recognition [14–17]. In the present study, MRA with a 3-tesla system showed superior performance compared with CTA. However, we consider that the performance of MRA would be lower with a 1.5-tesla MR system. While MRA is used for follow-up studies of coiled aneurysms, it is generally agreed that long-term angiographic monitoring is mandatory for these aneurysms [18,19]; it is also reported that high-resolution MRA is more sensitive to residual flow than is DSA [20,21]. Therefore, we consider that 3-tesla MRA is an ideal non-invasive imaging examination for investigating whether a branch vessel arises from an intracranial aneurysm sac, in screening imaging and in follow-up studies.

The greater accuracy of MRA for branch vessel detection is due to two factors: (1) the contrast-to-noise ratio of MRA is higher than that of CTA, as seen in case 1 of the present study (Fig. 1); and (2) the presence of perivascular structures impairs the detection of branch vessels on CTA, as seen in cases 2–4 (Figs. 2–4). On CTA, background noise obscures the signal from branch vessels in the case that signal fluctuation from background noise is greater than the signal from the vessel. The contrast-to-noise ratio of CTA images can be improved by increased radiation dose, but a higher radiation dose increases cancer risk. MRA therefore has particular merit for repeated examinations performed in the follow-up period because it delivers no radiation to the patient. There are concerns regarding the long-term health effects of ionizing radiation exposure [22,23], to the extent that the radiation dose of radiologic screening procedures will receive much more scrutiny in the future [24,25]. In addition, non-contrasted time-of-flight MRA has no risk of nephrotoxicity from the intravenous injection of contrast agent that is necessary in CTA.

While the results of previous studies indicate that MRA and CTA have similar overall accuracy for detecting intracranial aneurysms [9–11], the present results revealed the superior performance of MRA for detecting a branch vessel arising from an aneurysm sac. We consider that this inconsistency is caused by differences in the size of the targets: an aneurysm is much larger than a branch vessel arising from it. In the present study, the mean aneurysm size was 5.45 mm (range, 1.47–16.45 mm) and the mean branch vessel width was 0.99 mm (range, 0.47–1.99 mm). Detection performance is influenced by the signal contrast between the target and the surrounding structure. Because the partial volume effect is less for a large structure such as an aneurysm than for a small structure such as a branch vessel arising from the aneurysm, the signal contrast is more compromised for the smaller structure.

The major limitation of our report is that we used a CT protocol set for screening studies, which was not optimized for detection of a branch vessel arising from an intracranial aneurysm sac. The accuracy of the CTA studies could have been improved by optimizing the imaging protocol for this purpose; e.g., by increasing the tube voltage, the amount of contrast agent used, and the spatial resolution in image reconstruction. However, the MRA imaging protocol could also be optimized. For example, Willinek et al. [14] found

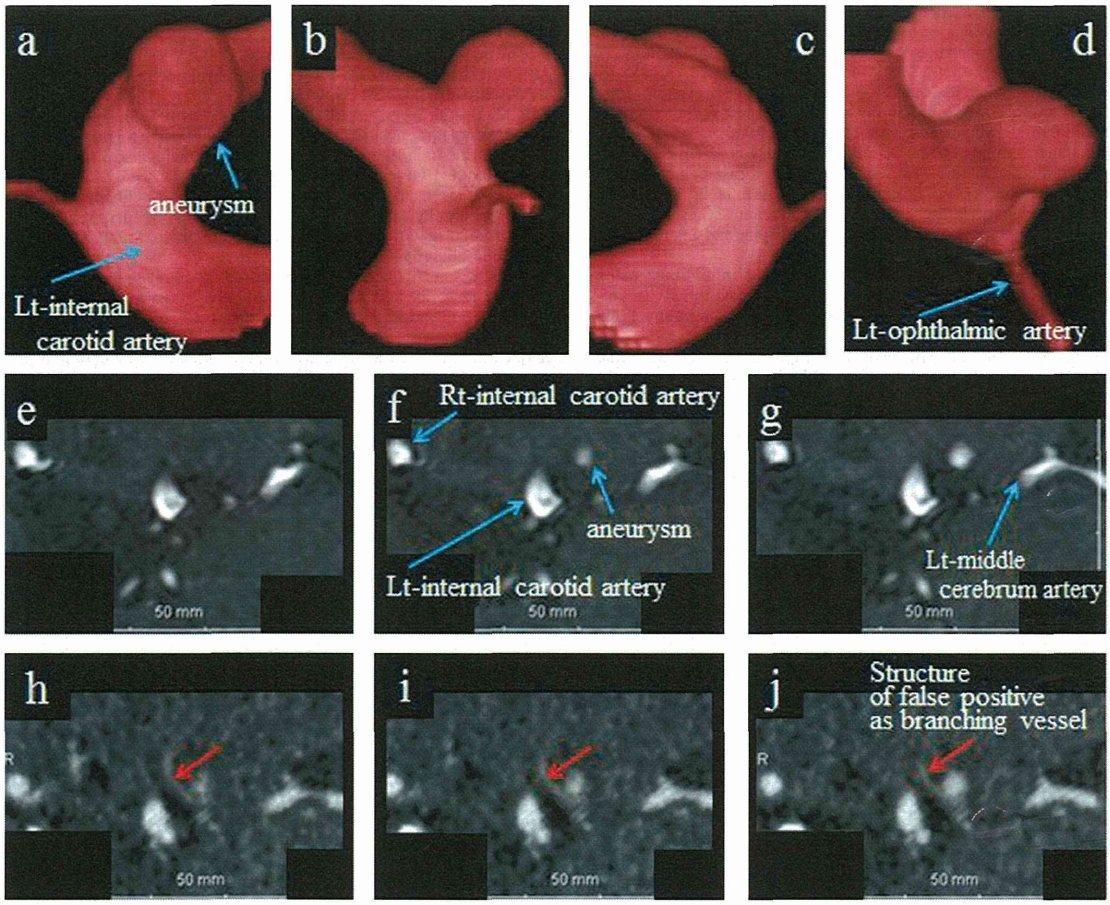

Fig. 4. False positive on 'CTA-VR + source images' and true negative on 'MRA-VR + source images' observed in patient 35. No branch vessel arising from the aneurysm sac was observed on VR-rotational DSA in this patient. (a)–(d) VR-rotational DSA (a: left lateral view, b: frontal view, c: right lateral view, and d: 90 °caudal rotation from front). (e)–(g) MRA source images. (h)–(j) CTA source images. The red arrow indicates a structure that was assessed as a branch vessel arising from the aneurysm sac but was in fact a vein. For subfigures (e)–(g) and (h)–(j), the image slices run superior to inferior, from left to right. (For interpretation of the references to color in this figure legend, the reader is referred to the web version of the article.)

that using high-spatial-resolution 3-tesla MRA improved the accuracy for detection of a branch vessel arising from an intracranial aneurysm sac. The present study reported the superior performance of 3-tesla MRA compared with CTA in screening imaging for detecting a branch vessel. Optimization of the MRA and CTA imaging protocols used to detect branch vessels arising from aneurysms is a topic for future study.

5. Conclusions

The results show that 3-tesla MRA is an ideal non-invasive imaging examination for detection of a branch vessel arising from an intracranial aneurysm sac. Higher accuracy, especially sensitivity, with MRA compared with CTA was found in ICA, but accuracy with MRA was same as that with CTA in MCA. This technique has particular value for observation of intracranial arteries in screening imaging and for follow-up studies because there is no radiation dose to the patient.

Acknowledgement

This study is supported by a Grant-in-Aid for Scientific Research on Innovative Areas (Comprehensive Brain Science Network) from the Ministry of Education, Science, Sports and Culture of Japan.

References

[1] Nakagawa T, Hashi K. The incidence and treatment of asymptomatic, unruptured cerebral aneurysms. J Neurosurg 1994;80:217–23.
[2] Ronkainen A, Miettinen H, Karkola K, Papinaho S, Vanninen R, Puranen M, et al. Risk of harboring an unruptured intracranial aneurysm. Stroke 1998;29:359–62.
[3] Juvela S, Porras M, Heiskanen O. Natural history of unruptured intracranial aneurysms: a long-term follow-up study. J Neurosurg 1993;79:174–82.
[4] Camarata PJ, Latchaw RE, Rufenacht DA, Heros RC. Intracranial aneurysms. Invest Radiol 1993;28:373–82.
[5] Wiebers DO, Whisnant JP, Huston 3rd J, Meissner I, Brown Jr RD, Piepgras DG, et al. Unruptured intracranial aneurysms: natural history, clinical outcome, and risks of surgical and endovascular treatment. Lancet 2003;362:103–10.
[6] Lubicz B, Lefranc F, Levivier M, Dewitte O, Pirotte B, Brotchi J, et al. Endovascular treatment of intracranial aneurysms with a branch arising from the sac. AJNR Am J Neuroradiol 2006;27:142–7.
[7] Castano-Duque CH, Ruscalleda-Nadal J, de Juan-Delago M, Guardia-Mas E, San Roman-Manzanera L, Bartomeus-Jene F, et al. Early experience studying cerebral aneurysms with rotational and threedimensional angiography and review of CT and MR angiography literature. Interv Neuroradiol 2002;8:377–91.
[8] Villablanca JP, Jahan R, Hooshi P, Lim S, Duckwiler G, Patel A, et al. Detection and characterization of very small cerebral aneurysms by using 2D and 3D helical CT angiography. AJNR Am J Neuroradiol 2002;23:1187–98.
[9] Ogawa T, Okudera T, Noguchi K, Sasaki N, Inugami A, Uemura K, et al. Cerebral aneurysms: evaluation with three-dimensional CT angiography. AJNR Am J Neuroradiol 1996;17:447–54.
[10] Preda L, Gaetani P, Rodriguez, Baena R, Di Maggio EM, La Fianza A, et al. Spiral CT angiography and surgical correlations in the evaluation of intracranial aneurysms. Eur Radiol 1998;8:739–45.

[11] Huston 3rd J, Nichols DA, Luetmer PH, Goodwin JT, Meyer FB, Wiebers DO, et al. Blinded prospective evaluation of sensitivity of MR angiography to known intracranial aneurysms: importance of aneurysm size. AJNR Am J Neuroradiol 1994;15:1607–14.
[12] Villablanca JP, Martin N, Jahan R, Gobin YP, Frazee, Duckwiler G, et al. Volume-rendered helical computerized tomography angiography in the detection and characterization of intracranial aneurysms. J Neurosurg 2000;93:254–64.
[13] Goto M, Kunimatsu A, Shojima M, Abe O, Aoki S, Hayashi N, et al. A pitfall of the volume rendering method with 3D time-of-flight MRA: a case of a branching vessel at the aneurysm neck. Magn Reson Med Sci 2013;12:53–6.
[14] Willinek WA, Born M, Simon B, Tschampa HJ, Krautmacher C, Gieseke J, et al. Time-of-flight MR angiography: comparison of 3.0-T imaging and 1.5-T imaging – initial experience. Radiology 2003;229:913–20.
[15] Sun ZK, Li YD, Li MH, Chen SW, Tan HQ. Detection of infundibula using three-dimensional time-of-flight magnetic resonance angiography with volume rendering at 3.0 tesla compared to digital subtraction angiography. J Clin Neurosci 2011;18:504–8.
[16] Murata T, Horiuchi T, Rahmah NN, Sakai K, Hongo K. Three-dimensional magnetic resonance imaging based on time-of-flight magnetic resonance angiography for superficial cerebral arteriovenous malformation – technical note. Neurol Med Chir 2011;51:163–7.
[17] Li MH, Li YD, Tan HQ, Gu BX, Chen YC, Wang W, et al. Contrast-free MRA at 3.0 t for the detection of intracranial aneurysms. Neurology 2011;77:667–76.
[18] Thornton J, Debrun GM, Aletich VA, Bashir Q, Charbel FT, Ausman J. Follow-up angiography of intracranial aneurysms treated with endovascular placement of Guglielmi detachable coils. Neurosurgery 2002;50:239–49 (discussion 249–250).
[19] Murayama Y, Nien YL, Duckwiler G, Gobin YP, Jahan R, Frazee J, et al. Guglielmi detachable coil embolization of cerebral aneurysms: 11 years' experience. J Neurosurg 2003;98:959–66.
[20] Majoie CB, Sprengers ME, van Rooij WJ, Lavini C, Sluzewski M, van Rijn JC, et al. Mr angiography at 3 T versus digital subtraction angiography in the follow-up of intracranial aneurysms treated with detachable coils. AJNR Am J Neuroradiol 2005;26:1349–56.
[21] Yamada N, Hayashi K, Murao K, Higashi M, Iihara K. Time-of-flight MR angiography targeted to coiled intracranial aneurysms is more sensitive to residual flow than is digital subtraction angiography. AJNR Am J Neuroradiol 2004;25:1154–7.
[22] Sodickson A, Baeyens PF, Andriole KP, Prevedello LM, Nawfel RD, Hanson R, et al. Recurrent CT, cumulative radiation exposure, and associated radiation-induced cancer risks from CT of adults. Radiology 2009;251:175–84.
[23] Griffey RT, Sodickson A. Cumulative radiation exposure and cancer risk estimates in emergency department patients undergoing repeat or multiple CT. AJR Am J Roentgenol 2009;192:887–92.
[24] Fazel R, Krumholz HM, Wang Y, Ross JS, Chen J, Ting HH, et al. Exposure to low-dose ionizing radiation from medical imaging procedures. N Engl J Med 2009;361:849–57.
[25] Lauer MS. Elements of danger – the case of medical imaging. N Engl J Med 2009;361:841–3.

Radiol Phys Technol (2015) 8:64–72
DOI 10.1007/s12194-014-0295-9

Longitudinal gray-matter volume change in the default-mode network: utility of volume standardized with global gray-matter volume for Alzheimer's disease: a preliminary study

Masami Goto · Osamu Abe · Shigeki Aoki · Naoto Hayashi · Hiroshi Ohtsu · Hidemasa Takao · Tosiaki Miyati · Hiroshi Matsuda · Fumio Yamashita · Takeshi Iwatsubo · Harushi Mori · Akira Kunimatsu · Kenji Ino · Keiichi Yano · Kuni Ohtomo

Received: 23 June 2014 / Revised: 4 September 2014 / Accepted: 5 September 2014 / Published online: 27 September 2014
© Japanese Society of Radiological Technology and Japan Society of Medical Physics 2014

Abstract Our aim was to show whether sensitivity for detecting volume changes in regional gray matter in default mode network (DMN) at converted [from mild cognitive impairment to Alzheimer's disease (from MCI to AD)] phase was improved by use of a standardized volume with global gray-matter volume. T1-weighted MR images (T1WI) of seven normal subjects and seven converted (from MCI to AD) patients were obtained from the Alzheimer's Disease Neuroimaging Initiative (ADNI) database. Gray-matter images segmented with Statistical Parametric Mapping 5 were measured by the atlas-based method. We focused on five nodes of the DMN. For each phase, region of interest (ROI) volumes in the five nodes were standardized by two methods: (1) the ratio to the screening phase (S_volume) and (2) the ratio to the screening phase after both volumes were standardized by the global gray-matter volume (S_N_volume). Significant group differences between longitudinal gray-matter volume change of the converted (from MCI to AD) group and that of the normal group were found in lateral temporal cortex by S_N_volume, and precuneus by S_N_volume. These findings are useful for improving the understanding of DMN volume changes at the converted (from MCI to AD) phase.

Keywords Aging · Brain volume · Central nervous system · Default mode network · Magnetic resonance imaging

For the Alzheimer's Disease Neuroimaging Initiative.
Data used in preparation of this article were obtained from the Alzheimer's Disease Neuroimaging Initiative (ADNI) database (adni.loni.ucla.edu). As such, the investigators within the ADNI contributed to the design and implementation of the ADNI and/or provided data but did not participate in the analysis or writing of this report. A complete listing of ADNI investigators can be found at: http://adni.loni.ucla.edu/wp-content/uploads/how_to_apply/ADNI_Acknowledgement_List.pdf.

M. Goto (✉) · K. Ino · K. Yano
Department of Radiological Technology, University of Tokyo Hospital, 7-3-1 Hongo, Bunkyo-ku, Tokyo 113-8655, Japan
e-mail: car6_pa2_rw@yahoo.co.jp

O. Abe
Department of Radiology, Nihon University School of Medicine, Chiyoda, Japan

S. Aoki
Department of Radiology, Juntendo University, Bunkyo-ku, Japan

N. Hayashi
Department of Computational Diagnostic Radiology and Preventive Medicine, University of Tokyo Hospital, Tokyo, Japan

H. Ohtsu
Department of Clinical Bioinformatics, University of Tokyo Hospital, Tokyo, Japan

H. Takao · H. Mori · A. Kunimatsu · K. Ohtomo
Department of Radiology, University of Tokyo Hospital, Tokyo, Japan

T. Miyati
Graduate School of Medical Science, Kanazawa University, Kanazawa, Japan

H. Matsuda
Department of Nuclear Medicine, Saitama Medical University International Medical Center, Saitama, Japan

1 Introduction

Resting-state functional magnetic resonance imaging (RfMRI) has rapidly become the target of advanced research in brain function studies [1]. RfMRI is a noninvasive technique used for investigating and characterizing in vivo the spontaneous correlations of blood-oxygen-level-dependent (BOLD) signals within and between different regions of the brain. RfMRI is an important diagnostic tool for evaluating brain function and neuronal connectivity. Previous reports of resting-state functional connectivity suggest the existence of at least three canonical networks [2–5]. The first, termed the central executive network, comprises the dorsolateral prefrontal cortex and posterior-parietal cortex and is also considered crucial for maintenance and processing of information in the working memory. The second, termed the salience network, includes the anterior cingulate cortex and fronto-insular cortex, which are combined as the ventrolateral prefrontal cortex and anterior insula. The third system, termed the default mode network (DMN), combines the posterior cingulate cortex, precuneus, lateral temporal cortex (LTC), medial prefrontal cortex (MPFC), and inferior parietal lobule (IPL). Analysis of low-frequency spontaneous BOLD fluctuations enables RfMRI to detect resting-state synchronization in the functional network of these regions [2, 6–9]. Because this network is typically deactivated during external stimulation, it has been termed the DMN.

Many studies have investigated the behavioral function of the DMN. The role of the DMN is to optimize performance by allocating resources to task-related regions and away from task-irrelevant structures [10]. It has been suggested that the DMN is involved in the processes of self-referential mental activity and introspectively oriented mode [11] and that it plays a role in attending to environmental stimuli as well as mediating processes such as reviewing past knowledge and preparing future actions. It may also be involved in episodic memory [12].

Interestingly, the DMN regions comprise the typical predilection sites of Alzheimer's disease (AD) [13], the most frequent cause of dementia in the elderly and the most common neurodegenerative disorder in humans. Early symptomatology for AD has been linked to changes in the DMN, based on glucose metabolism and blood flow positron emission tomography and single photon emission computed tomography measurements [14]. RfMRI has identified significant disruptions in DMN co-activation in patients with AD [12, 15]. In addition, RfMRI is a noninvasive and radiation-exposure-free biomarker of early AD [12]. As a result, the DMN has rapidly become the target of extensive research in the AD field [14, 16–20].

However, to the best of our knowledge, estimation of subdivided DMN volume in normal and converted [from mild cognitive impairment to Alzheimer's disease (from MCI to AD)] groups has not been reported in previous studies. We can estimate the gray-matter volume of the DMN by the atlas-based method using segmented gray-matter images from magnetic resonance (MR) T1-weighted images (T1WI) [21]. Therefore, our aim in the present study was to show whether the sensitivity for detecting volume changes of regional gray matter in DMN at the converted (from MCI to AD) phase was improved by use of standardized volume with global gray-matter volume compared with another method in the atlas-based method.

2 Materials and methods

2.1 Subjects

Data used in the preparation of this article were obtained from the Alzheimer's Disease Neuroimaging Initiative (ADNI) database (adni.loni.ucla.edu). The ADNI was launched in 2003 by the National Institute on Aging, the National Institute of Biomedical Imaging and Bioengineering, the Food and Drug Administration, private pharmaceutical companies, and non-profit organizations, as a $60 million, 5-year public–private partnership. The primary goal of the ADNI has been to test whether serial MRI, positron emission tomography (PET), other biological markers, and clinical and neuropsychological assessment can be combined for measurement of the progression of MCI and early AD. Determination of sensitive and specific markers of very early AD progression is intended to aid researchers and clinicians to develop new treatments and monitor their effectiveness, as well as lessen the time and cost of clinical trials.

ADNI is the result of efforts of many co-investigators from a broad range of academic institutions and private corporations, and subjects have been recruited from more than 50 sites across the US and Canada. The initial goal of ADNI was to recruit 800 adults, ages 55–90 years, to participate in the research, with approximately 200 cognitively normal older individuals to be followed for 3 years, 400 people with MCI to be followed for 3 years, and 200 people with early AD to be followed for 2 years. (For up-to-date information, see http://www.adni-info.org.)

We downloaded data on two groups: a normal group and a converted (from MCI to AD) group, from the ADNI

F. Yamashita
Department of Radiology, National Center Hospital of Neurology and Psychiatry, Tokyo, Japan

T. Iwatsubo
Department of Neuropathology, University of Tokyo, Tokyo, Japan

Table 1 Characteristics of participants in the present study (from the ADNI database)

Group type	Converted phase (months)	Gender	Age on screening (years)	Education (years)
MCI to AD	18	Female	71.0	14
MCI to AD	12	Male	79.8	18
MCI to AD	12	Female	72.0	16
MCI to AD	12	Male	75.8	13
MCI to AD	12	Female	79.8	16
MCI to AD	12	Male	72.2	18
MCI to AD	18	Female	71.1	18
Normal	–	Female	71.0	14
Normal	–	Male	80.9	18
Normal	–	Female	71.2	16
Normal	–	Male	76.6	14
Normal	–	Female	80.3	18
Normal	–	Male	72.6	18
Normal	–	Female	70.6	18

Data (i.e., cognitive function test scores and MRI) for all subjects in the present study were obtained at each visit phase (at screening and at 6, 12, 24, 36, and 48 months). Subjects with MCI visited at 18 months additionally. The converted phase means phase at conversion from MCI to AD. Included in the converted and normal groups were subjects with matching gender, age, and years of education period

Table 2 Cognitive function test scores of groups in the present study (from the ADNI database)

Test	Group	Visit phase						
		Screening	6 months	12 months	18 months	24 months	36 months	48 months
NMSE	Converted	27.7 ± 1.8	26.1 ± 2.3	25.7 ± 2.8	24.9 ± 3.0	24.4 ± 3.3	24.6 ± 3.9	22.6 ± 1.85
	Normal	29.4 ± 0.8	29.5 ± 0.5	29.4 ± 1.1	–	29.2 ± 1.1	29.8 ± 0.4	29.5 ± 0.8
CDR	Converted	0.5 ± 0	0.5 ± 0	0.57 ± 0.19	0.79 ± 0.27	0.79 ± 0.27	1.33 ± 0.82	0.90 ± 0.27
	Normal	0 ± 0	0 ± 0	0 ± 0	–	0 ± 0	0 ± 0	0 ± 0
ADAS-cog	Converted	13.9 ± 5.4	15.8 ± 5.5	14.6 ± 5.3	16.4 ± 6.6	16.3 ± 4.1	16 ± 4.7	21.6 ± 5.5
	Normal	6.9 ± 2.1	6.1 ± 3.8	6.3 ± 2.7	–	6.4 ± 3.4	5.7 ± 2.3	6.8 ± 2.2

Values are presented as the mean ± standard deviation

MMSE mini-mental state examination, *CDR* clinical dementia rating, *ADAS-cog* Alzheimer's Disease Assessment Scale-cognitive subscale

database. The ADNI database includes several hundred subjects in each group (i.e., normal, MCI, and AD). However, public data in the converted (from MCI to AD) group in the ADNI includes only 16 subjects. In addition, subjects with deficit data (i.e., deficit on 3D-T1WI or deficit on cognitive function tests) were excluded from this study. As a result, used data as converted (from MCI to AD) group were 7 subjects. We then set up these two groups of subjects in whom three factors (gender, age, and education period) were matched between the normal and the converted (from MCI to AD) group. The characteristics of these groups are summarized in Tables 1 and 2. Table 1 shows individual information (converted phase, gender, age, and education period) on the matched participants in our study (from the ADNI database). The converted phase means phase at conversion from MCI to AD. Table 2 shows cognitive test scores of the matched groups in our study (from the ADNI database). The 3D-T1WIs for all subjects in the present study were obtained by a 1.5 Tesla scanner at each visit phase (at screening and at 6, 12, 24, 36, and 48 months). Subjects with MCI visited at 18 months additionally. Details on the MRI scanning protocol are indicated in the ADNI database. The MRI scanning protocols are identical for each subject.

2.2 Image processing for brain tissue segmentation

We used Statistical Parametric Mapping 5 (SPM5) [22] software (Wellcome Department of Imaging Neuroscience Group, London, UK; http://www.fil.ion.ucl.ac.uk/spm). The 3D-T1WIs in native space were bias-corrected, spatially normalized, and segmented into gray matter, white matter, and cerebrospinal fluid images. The voxel size was set to $2 \times 2 \times 2$ mm^3 for the spatially normalized images

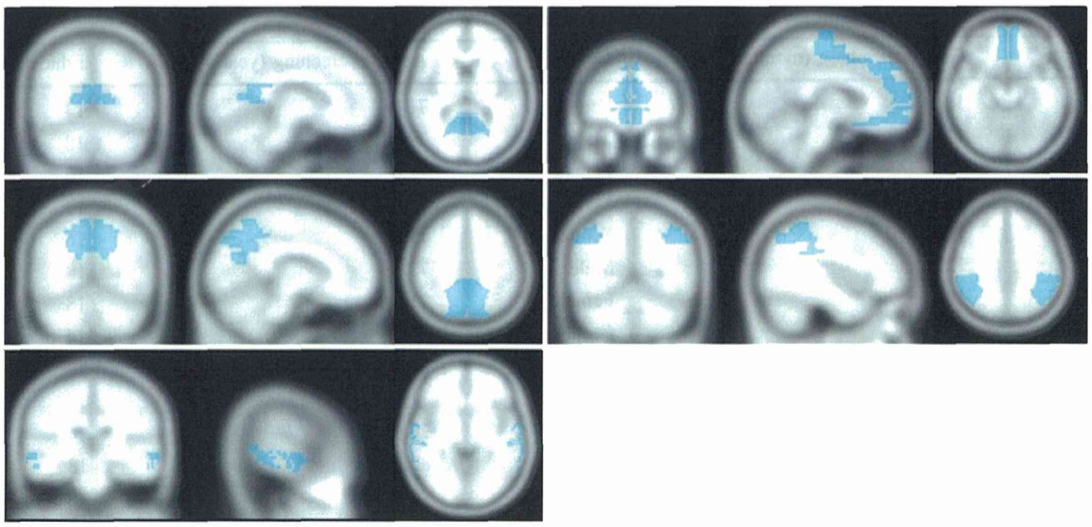

Fig. 1 ROIs superimposed on T1 template images. We used the following ROIs: posterior cingulate (*top left*), precuneus (*middle left*), lateral temporal cortex (LTC) (*bottom left*), medial prefrontal cortex (MPFC) (*top right*), and inferior parietal lobule (IPL) (*middle right*)

and was set as the default on SPM5 for other images. The parameters of SPM5 were identical in analyses for all T1WIs.

2.3 Atlas-based volume measurement method and statistical analysis

Regions of interest (ROI) for gray-matter volume measurement of the DMN were obtained by WFU PickAtlas [21]. This program automatically generates segmented atlas ROI templates in Montreal Neurological Institute (MNI) space [23]. The ROIs defined in the atlas were originally based on manual drawing of the borders of brain regions according to the Talairach atlas [21]. Figure 1 shows the placement of ROIs in the following five DMN regions: posterior cingulate, precuneus, LTC, MPFC, and IPL [14, 16–18, 20]. ROI volume measurements were performed on spatially normalized gray-matter images for each of the five regions. ROI volumes were calculated by 'number of voxel in the ROI' × 'tissue existence probability'. Brain shapes were normalized to MNI space, and intensity modulation step was included in this normalization process. Then, the spatially normalized gray-matter images have information of tissue existence probability. The gray-matter volumes can be calculated from tissue existence probability. ROI volumes were measured bilaterally in all subjects. ROI volumes for the five regions were standardized in each phase by two methods: 1) the ratio to the screening phase (S_volume) and 2) the ratio to the screening phase after both volumes were standardized by the global gray-matter volume (S_N_volume). S_volume and S_N_volume were defined by the following formulae:

$$\text{S\_volume} = \frac{\text{ROI volume on each phase}}{\text{ROI volume on screening phase}}$$

$$\text{S\_N\_volume} = \frac{(\text{ROI volume/global gray matter volume}) \text{ on each phase}}{(\text{ROI volume /global gray matter volume}) \text{ on screening phase}}$$

The global gray-matter volume was measured by SPM5.

Two-way repeated measure analysis of variance (two-way repeated ANOVA) was used to test for group differences (the independent variable is group, and the dependent variable is visit phase) in S_volume and S_N_volume in each of the five ROIs between the normal group and the converted (from MCI to AD) group. Significant difference was defined as $p < 0.1$.

3 Results

Two-way repeated ANOVA revealed significant group differences in the LTC for S_N_volume (more progressive value reduction of S_N_volume in the converted (from MCI to AD) group compared with the normal group) and in the precuneus for S_N_volume (more progressive value increase of S_N_volume the converted (from MCI to AD) group compared with the normal group). No significant group differences in other ROIs for S_N_volume and in all ROIs for S_volume were found. The trend of visit-phase-related volume change is shown in Fig. 2.

4 Discussion

In the present study, significant group differences were observed in regional volumes for S_N_volume, but not for

S_volume. For example, the LTC of the converted (from MCI to AD) group showed progressive value reduction of S_N_volume (see the left-side panel of the LTC in Fig. 2), while there appeared to be more progressive value increase of S_N_volume in the precuneus of the converted (from MCI to AD) group (see the left-side panel of the precuneus in Fig. 2) than in the normal group. Therefore, our results suggest that S_N_volume is more sensitive than S_volume for detecting atrophy. S_N_volume is corrected for individual differences in the speed of global brain atrophy (i.e., a high S_N_volume value indicates that the reduction in ROI volume is less rapid than that in global gray matter, while a low S_N_volume value indicates that the reduction in ROI volume is more rapid than that in global gray matter). In other words, more progressive value increase of S_N_volume in the precuneus of the converted (from MCI to AD) group than in the normal group does not mean volume increase of the precuneus; it means that the reduction in the volume of precuneus in the converted (from MCI to AD) group is less rapid than that in the global gray matter compared with the normal group. In contrast, S_volume is not corrected for individual differences in the speed of global brain atrophy. That is, S_N_volume is influenced by 'cortex atrophy in AD effect', and S_volume is influenced by 'cortex atrophy in AD effect' and 'cortex atrophy in aging effect' [24–27]. Standard deviations were generally larger in S_volume than in S_N_volume, probably because S_volume includes individual differences in aging effect (see Fig. 2). This difference in the variation of data points between S_volume and S_N_volume may explain why S_N_volume is more sensitive than S_volume for detecting brain atrophy in the DMN.

In many previous reports, a significantly reduced gray-matter volume was observed in the LTC of AD patients (compared with controls) [26–29]. In addition, in comparing AD patients with controls, Frisoni et al. [30] reported that the largest atrophic regions (i.e., largest significant cluster size) corresponded to the hippocampal cortex while smaller atrophic regions (i.e., smaller significant cluster size) were found in the temporal and cingulate gyri. Based on these lines of evidence, it is widely accepted that atrophy is more progressive in the LTC of patients with AD and MCI compared with that in normal subjects.

In the present study, volume reduction in the LTC of the converted (from MCI to AD) group was more progressive compared with that of the normal group in terms of S_N_volume.

It appears to be an error of brain volume analysis that the atrophy speed of the precuneus in the converted (from MCI to AD) group was slower than that of the normal group. However, two previous studies showed increased cortical thickness in the precuneus of an asymptomatic MCI group compared with a control subject group and suggested that this increment in cortical thickness could be related to reactive neuronal hypertrophy and/or inflammation driven by amyloid in the very early stages of the disease [31, 32]. Therefore, we hypothesize that the less rapid volume loss in the precuneus of the converted (from MCI to AD) group in the present study could be related to reactive neuronal hypertrophy and/or to inflammation driven by amyloid.

Group differences between the normal group and the converted (from MCI to AD) group were not observed in the other three regions (posterior cingulate, medial prefrontal cortex, and inferior parietal lobule). However, the results must be interpreted with caution. Volume changes may not have been observed because of two factors: a small sample size and a small gray-matter volume change in the regions. We expect that volume changes would also have been observed in these three regions if we had used a large sample, because gray-matter volume reduction was observed in these three regions in previous studies [26–30]. In other words, in the present study, group differences between the normal group and the converted (from MCI to AD) group were larger in the LTC and precuneus than in the other three regions.

Early pathology observations have revealed that AD affects a subset of neurons in regional and laminar specific neuronal systems [33]. A disconnection syndrome occurs in AD, beginning with the entorhinal cortex, after which the disease gradually progresses in a stepwise fashion along cortico-cortical connections [34]. Large cross-sectional studies have revealed that cortical neurofibrillary tangle densities and amyloid deposition are associated with the severity of dementia, neuronal loss, and atrophy [35]. These pathology observations support the hypothesis that the DMN and its subsystems are affected early in AD and MCI. In fact, other previous studies have demonstrated a loss of functional connectivity in the DMN in AD and MCI [36, 37].

Petrella et al. [38] showed highest integrity in controls and lowest integrity in subjects with AD for fMRI-measured DMN connectivity using goodness-of-fit indices. Although an association between AD and the DMN is of great interest, there are few reports on DMN gray-matter volume in AD patients. One previous report [38] found a significant difference in gray-matter probability in the DMN among four groups. When individual brain shapes were transformed to MNI space by the spatial normalization process with intensity modulation, signals of voxel in the spatially normalized gray-matter images mean the gray-matter probability. The four groups were normal controls, MCI nonconverters, MCI converters, and AD patients, and the gray-matter probabilities were 0.453 ± 0.024, 0.441 ± 0.036, 0.415 ± 0.028, and 0.422 ± 0.047, respectively. However, this previous report did not discuss

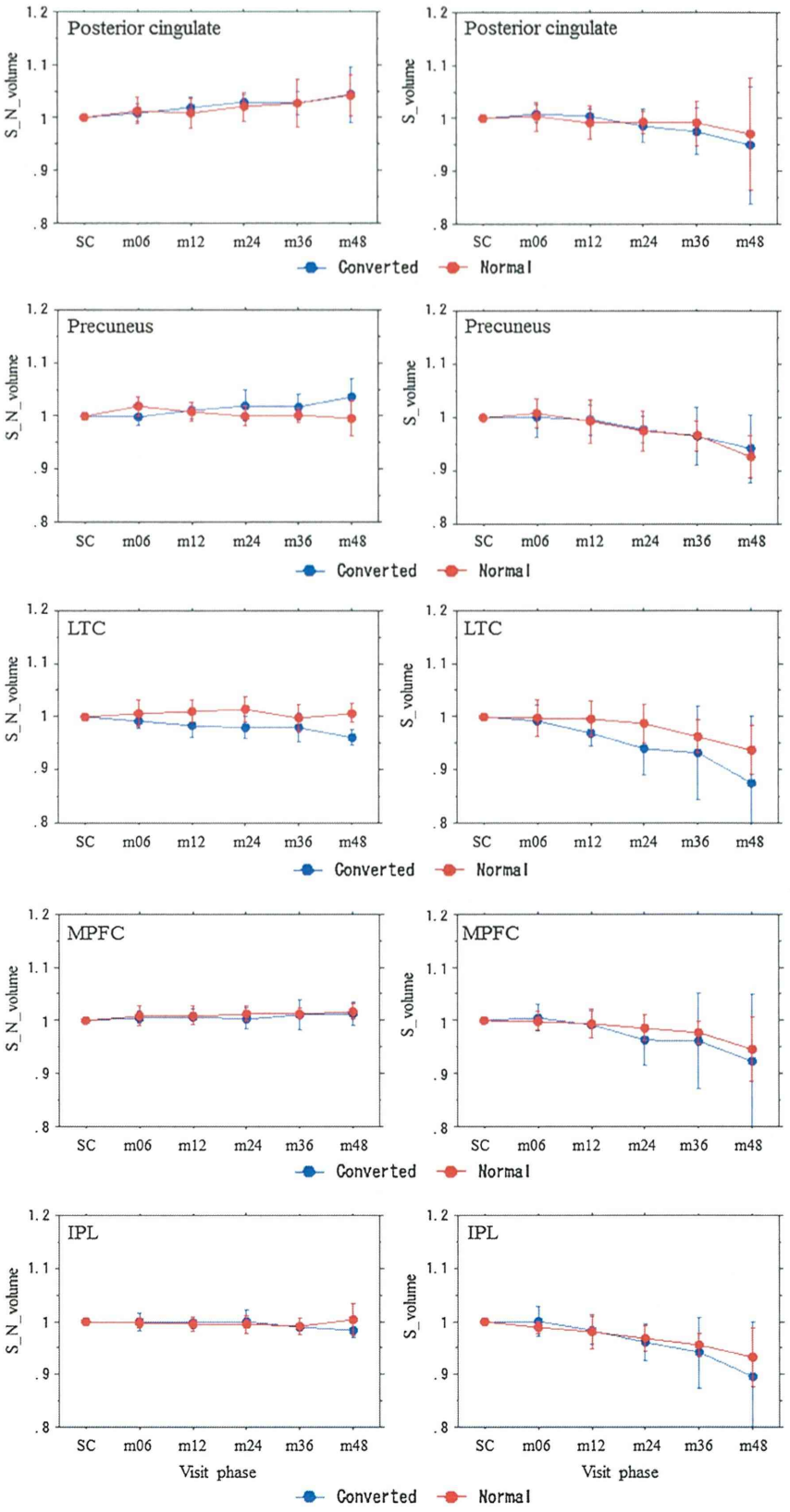

Fig. 2 Scatterplots of S_N_volume (*left side*) and S_volume (*right side*) according to visit phase. Two-way repeated ANOVA revealed significant group differences between the normal and converted (from MCI to AD) groups in the LTC for S_N_volume and in the precuneus for S_N_volume. S_volume is defined as the ratio to the screening phase; S_N_volume is defined as the ratio to the screening phase after both volumes were standardized by global gray-matter volume (see formulae in the Sect. 2). Visit phase is shown on the horizontal axes [at screening and at 6, 12, 24, 36, and 48 months (m)]. The ROI names are indicated on the respective plot areas. The mean of the standardized value in the normal (*red*) and converted (from MCI to AD) groups (*blue*) is shown with the respective standard deviation

the gray-matter volumes of the subdivided DMN. To the best of our knowledge, subdivided DMN volume changes in normal and AD groups are reported for the first time in the present report.

The hippocampus is integral to episodic memory processing [39]. Episodic memory loss is one of the cardinal features of AD [40] and the medial temporal lobe is among the first areas affected by pathology in AD [41]. The hippocampus has a key role in cognitive function. However, the hippocampus is relatively small, resulting in ROI placement being error prone. In addition, the bilateral hippocampus had the lowest associations with other regions of the DMN in both young and old cohorts [42], and numerous studies regarding hippocampal volume change in normal and AD subjects are reported. Therefore, we did not use a hippocampal ROI in the present study.

When gray-matter volume is measured in areas of the DMN defined by RfMRI, care must be taken regarding the following three factors:

1. Previous studies showed that control by the gray-matter volume in each voxel is important in RfMRI because the signal is influenced by aging [43–45]. Activity expressed in resting-state networks was decreased (that is, a lower BOLD signal change was observed) in older compared with younger subjects. These results were influenced by correction with the gray-matter volume index within the areas of these resting-state networks. In addition, age effects are reported in several other brain regions with normal aging by RfMRI (increased parietal and decreased hippocampal activation [46, 47], increased [48] and also decreased [49] anterior cingulate cortex activation, decreased deactivation of the medial parietal/posterior cingulate region [50], and decreased activation of a large part of the frontal and/or parietal brain areas [51]). Accelerated atrophy is also reported in the posterior cingulate gyrus, one of the core regions of the DMN [52] and an area with the earliest decline in glucose utilization in the preclinical stages of AD [53].
2. The defined area of the DMN varies between RfMRI methods because of differences in analytical procedure among the various methods. Koch et al. [42] reported that effects of normal aging such as loss of the posterior cingulate cortex co-activity could be detected by independent component analyses, but not by signal time course correlation analyses of DMN interconnectivity.
3. Marek et al. [54] reported diurnal changes in the neuronal activity level of resting-state networks.

When reports regarding the gray-matter volume of the DMN are compared the influence of factors 1–3 may confuse our understanding of the phenomenon, whereas in contrast, DMN areas defined by use of the atlas-based method are generally consistent between reports. Therefore, when reports regarding gray-matter volume of the DMN are compared, the confusion factor is reduced in the atlas-based method compared with when RfMRI is used. However, we must be mindful that the DMN defined by the atlas-based method is not the true area of the DMN in the individual.

We used the voxel size as $2 \times 2 \times 2$ mm^3. If image with $2 \times 2 \times 2$ mm^3 was used as structural image, partial volume effect is an important problem. In addition, using smaller voxel size may improve the accuracy for brain volumetry with the spatial normalized gray-matter image. However, previous studies commonly used approximately $2 \times 2 \times 2$ mm^3. In our other study, we showed that variation of spatial resolution changed a result of brain volumetry. Therefore, if we want to compare the present report with previous reports, we need to use same voxel size between the present study and previous study.

A main limitation of the present study is that the DMN regions were defined by the atlas-based method rather than the RfMRI method. Unfortunately, because fMRI was not performed by ADNI on the participants in the present study, we are unable to infer individual DMN regions. A common definition of the DMN area was used, based on many reports [14, 16–18, 20]. We employed five nodes of the DMN based on the definitions provided in these reports. When gray-matter volume is measured in areas of the DMN defined by RfMRI, care must be taken regarding the three factors mentioned. Therefore, we think that estimates of gray-matter volume change with regions defined by RfMRI are complicatedness compared with atlas-based method as present study.

Another limitation is the small sample size (we used all public data of the converted (from MCI to AD) group in the ADNI (see the MATERIALS AND METHODS in the present report). The result of brain volumetry with MRI was influenced by many factors (i.e., image distortion, signal intensity non-uniformity of image, and signal-to-noise ratio) [55–58]. Further studies with a large sample size are required for validation of the present result. We expect that the ADNI data base provide more many data as converted (from MCI to AD) group.

The last limitation is the possibility of mis-registration in spatial normalization process and mis-segmentation in the gray-matter image. Volumetry with the normalized gray-matter image has this limitation. Therefore, we checked spatially normalized T1WIs and the gray-matter images, and we found not clearly mis-registration (i.e., mainly inversion of image-orientation) and mis-segmentation (i.e., mainly interfusion of the white matter). Group comparison method for volumetry with the spatially normalized gray-matter images was used many previous